## Supplementary materials

**Dynamic properties of mixed cationic/nonionic adsorbed layers at the n-hexane/water interface: Capillary pressure experiments under low gravity conditions**

G. Loglio [a,*], V.I. Kovalchuk [b], A.G. Bykov [c], M. Ferrari [a], J. Krägel [d], L. Liggieri [a], R. Miller [d], B.A. Noskov [c], P. Pandolfini [a], F. Ravera [a] and E. Santini [a]

[a] *Institute of Condensed Matter Chemistry and Technologies for Energy, 16149 Genoa, Italy*
[b] *Institute of Biocolloid Chemistry, 03142 Kiev, Ukraine*
[c] *Department of Colloid Chemistry, St. Petersburg State University, 198504 St. Petersburg, Russia*
[d] *Max Planck Institute of Colloids and Interfaces, 14424 Potsdam/Golm, Germany*

Appendix A

*Optical calibration in-flight check*

1.A.- *Procedure for capillary coating*

The capillary was coated with an oleophobic / hydrophobic film by using Acota Certonal FC-734 perfluoropolymer.

The coating process was performed according to the following four sequential steps

a.- Full immersion of the capillary into $CrO_3$ + $H_2SO_4$ (chromic mixture), gently stirring the liquid mixture during 10 minutes.

b.- Washing the capillary under flowing tap water, flushing and removing the chromic mixture from the external side and from the internal bore during about one minute. Subsequently, rinsing the capillary by dipping several times into a bath of twice-distilled water (the water trapped inside the capillary was removed each time by a nitrogen flow).

c.- Drying of the capillaries overnight, in an oven at 100 ℃ (the capillary was placed inside a glass beaker).

d.- Coating of the capillary by full immersion into a bath of Acota Certonal FC-734 perfloropolymer, during 20 seconds. After evaporation of the solvent (by flowing externally and internally a slow nitrogen stream), the operation is repeated a second time.

2.A- *Detection of capillary diameter and of drop profile*

In the course of the experiment time-line, about eighty-thousand time-tagged 1000x1000-pixel drop images, sampled at 35-second intervals, were telemetered in concomitance with the downlink transmission stream of the data packets. Visual inspection of the drop behavior, in contact with the capillary tip, and of possible objectionable items inside the field of view were the principal aims of the telemetered images. In addition, such images allowed the in-flight check of the optical calibration, at certain statistically-selected instances during the time-line.

For the purpose of an in-flight calibration check, the images were contrast enhanced, properly adjusting the grey-level distribution, by a dedicated software for image processing. Actually the visualisation of the interface profile, separating the two adjoining liquid phases, is a critical item (in particular the difference of the standard refractive indexes between hexane and water is very small,

that is, $\Delta n = 1.375 - 1.333 = 0.042$, while the difference between fused-quartz capillary and water is $\Delta n = 1.458 - 1.333 = 0.125$).

Fig. S1a shows an example of the detection of capillary diameter and of drop profile for a 1000x1000-pixel drop image acquired during an oscillation experiment. The capillary diameter and the cap-shaped drop edge was acquired in pixel units by discrimination at the 128-grey-level, using a sub-pixel resolution procedure.

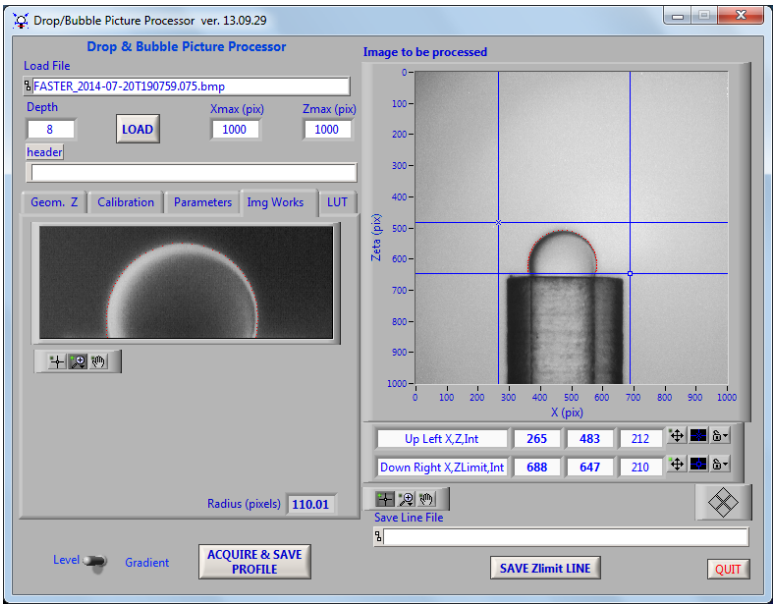


Fig. S1a.- Detection of capillary diameter and of drop profile for a 1000x1000-pixel drop image acquired during an oscillation experiment (specifically, temperature T= 20 ℃, injection 5-1, amplitude A = 20% , frequency f = 0.08 Hz). Image magnification = 2.5x. Image time-tag value = 2014-07-20 19:07:59.075.

Fig. S2a shows an example of the detection of capillary diameter and of drop profile for a 1000x1000-pixel drop image acquired during a growing drop experiment. The capillary diameter and the cap-shaped drop edge was acquired in pixel units by a grey-level gradient algorithm, using a sub-pixel resolution procedure.

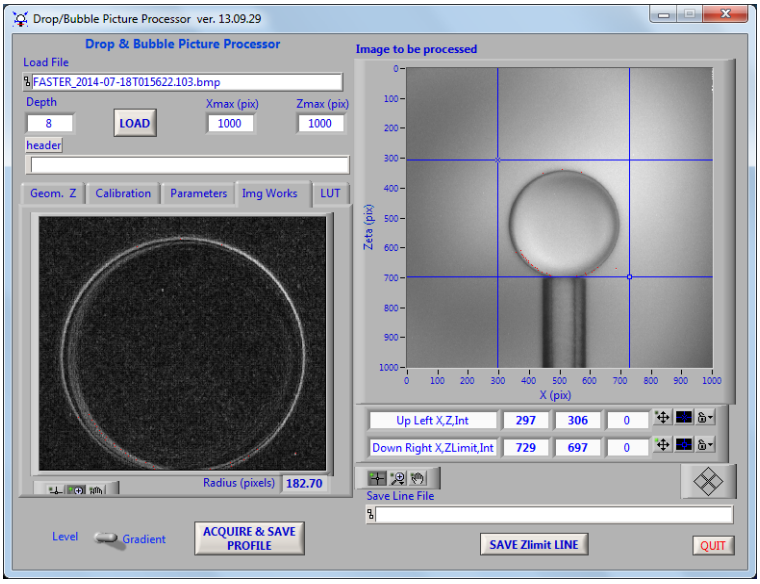


Fig. S2a.- Detection of capillary diameter and of drop profile for a 1000x1000-pixel drop image acquired during a growing drop experiment (temperature T= 20 ℃, injection 4-1). Image magnification = 1.0x. Image time-tag value = 2014-07-18 01:56:22.103.

The knowledge of the capillary diameter, d = 0.984 mm, allowed the stability of the on-ground optical calibration parameters to be confirmed (namely, for 2.5x-optical magnification c = 2.583 μm/pix and for 1.0x-optical magnification c = 6.515 μm/pix). Together with the calibration assessment, the drop-edge detection enabled the transformation from pixels to Cartesian co-ordinates of the drop profile points and hence the determination of the geometrical properties of the drop in SI-units.

3.A- *Drop geometrical properties: comparison between intermittent one-second packets*

Sequences of one-second time-tagged packets, each one containing twenty 33-point drop profiles and the capillary reference points, were telemetered in intermittent mode with the main one-second time-tagged packets, containing all the experimental geometrical and physical properties.

A dedicated software allows the conversion of the acquired pixel points (telemetered in arbitrary digital units) into SI-unit geometrical properties, persisting with the confirmed optical calibration parameters. The Fig. S3a shows an example of such an implemented tool, where the spherical cap-shaped drop and the capillary tip are also visualized.

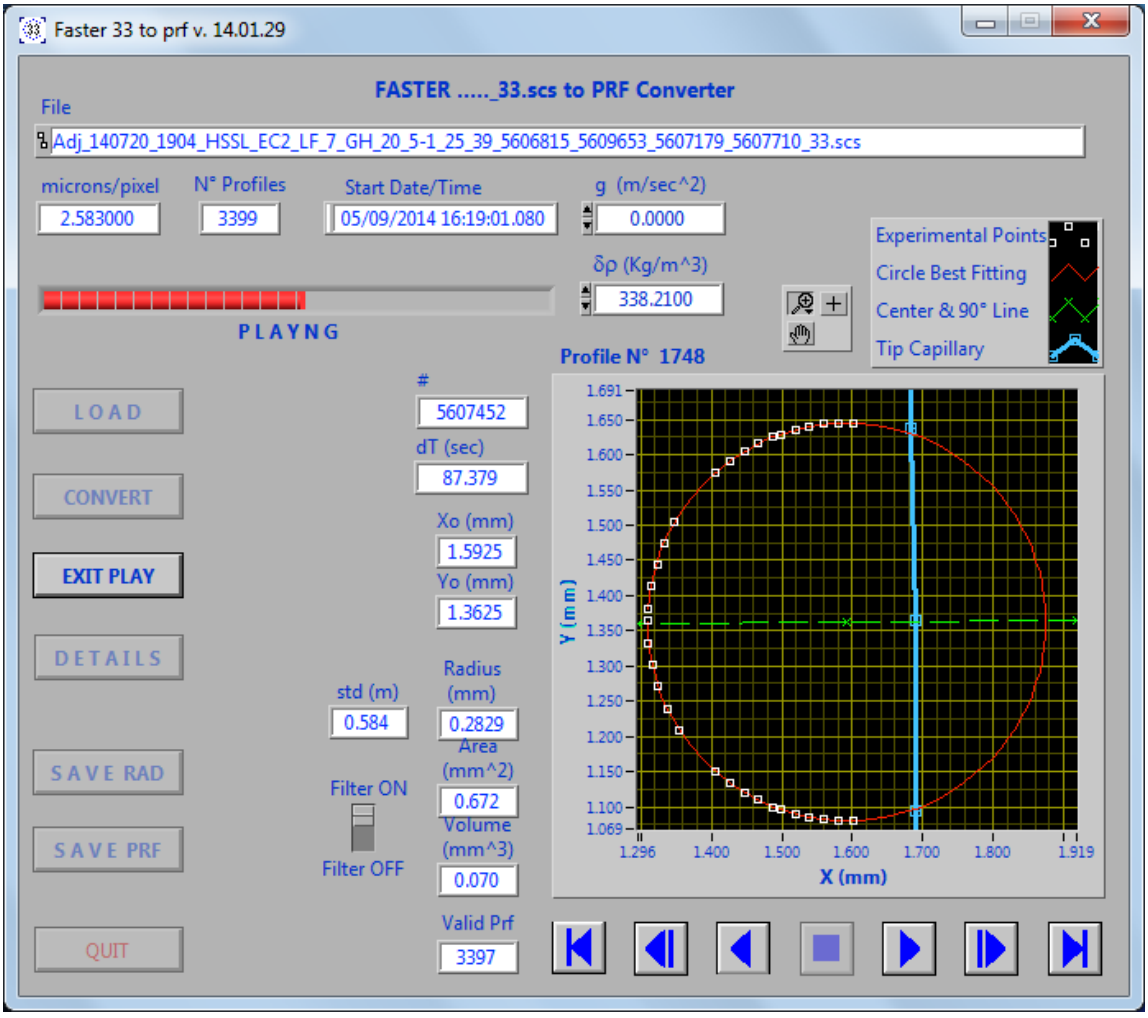


Fig. S3a.- Example of a 33-point drop profile, with the reference capillary points.

The Fig. S4a, as an example, illustrates a comparison of geometrical properties, in particular the radius values are here plotted (that is, the telemetered 3-point radius values are plotted on the left axis while the drop radius values, determined from the 33-point drop profile, are plotted on the right axis). The plot reports a selected part of an 8-frequency oscillation experiment in the injection 5-1 sample.

As seen in Fig.4a, the radius values, obtained from different telemetered sources, compare very satisfactorily, hence constituting a consistent set of experimental data. Actually all other geometrical drop properties compare in a similar fashion.

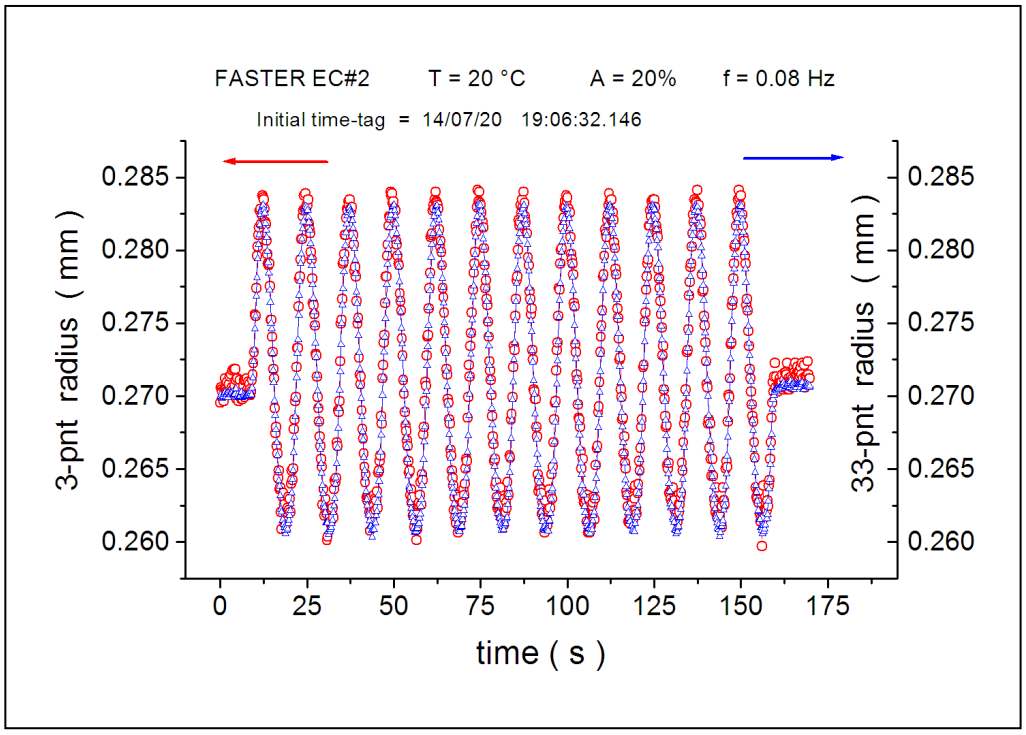


Fig. S4a.- Comparison of radii for an oscillating drop at frequency f= 0.08 Hz, amplitude A = 20%, temperature T = 20 ℃. Left axis, red points, telemetered 3-point radii, Right axis, blue points, drop radii determined from the 33-point drop profile. The origin of the time axis is arbitrarily taken at the initial time-tag of the start one-second packet for the 0.08-Hz experiment portion. Packet time-tag value = 14/07/20 19:06:32.146 .

Appendix B

*Adjustment of pressure sensor calibration*

The offset-parameter value of the pressure-sensor calibration is inherent in the specific offset value of the pressure-sensor device and in the additional offset-value of the electronic measurement chain. As the total value is sensitive to temperature and mechanical stresses, the accurate in-flight adjustment of such parameter is fundamental for the interpretation of the experimental results and for their quantitative analysis.

According to the Gauss-Laplace principle, the offset adjustment value is determined by the linear fit of a differential-pressure vs. inverse-radius plot, at constant interfacial tension, obtained during the ramp interval of a growing drop experiment. The intercept with the pressure axis is adjusted to cross the axis origin.

In case a sample containing pure liquids is not available, samples with greatest surfactant concentration are privileged for the study of growing drop experiments, as the interfacial tension relaxation overwhelms the interfacial area expansion during the entire ramp interval.

Fig. S1b illustrates an example for a growing drop experiment, selected for the in-flight pressure calibration at temperature T = 20 ℃, for a sample at the injection 6-5.

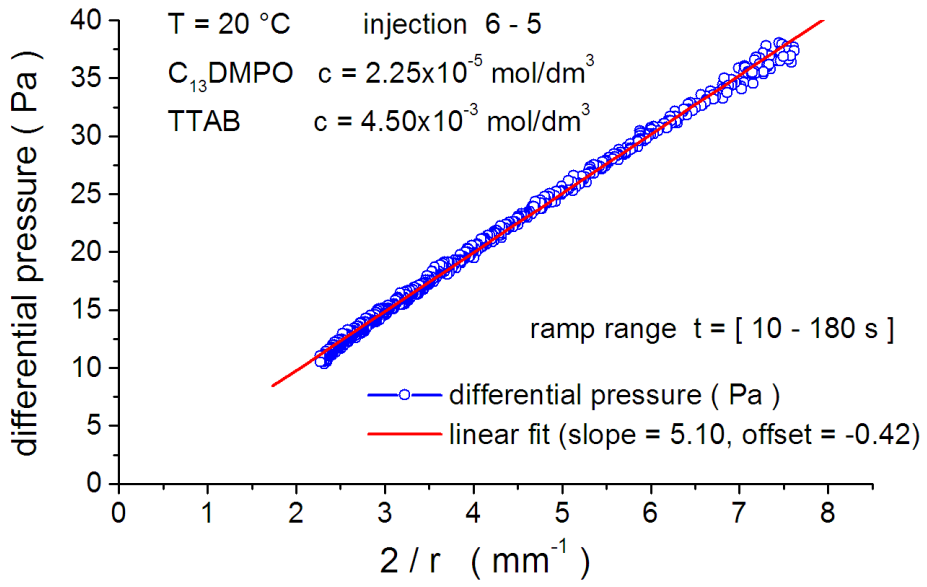


Fig. S1b.- Fitting of differential pressure vs. inverse radius data for injection 6-5 at T = 20 ℃ for a growing drop experiment, with filtered reference pressure and adjusted calibration parameters.

The Fig. S2b shows the behaviour of the interfacial tension for the growing drop experiment of Fig. S1b, including the pre-ramp and post-ramp time. As seen, during the ramp the interfacial tension is almost constant around $\gamma$ = 4.8 -4.9 mN/m .

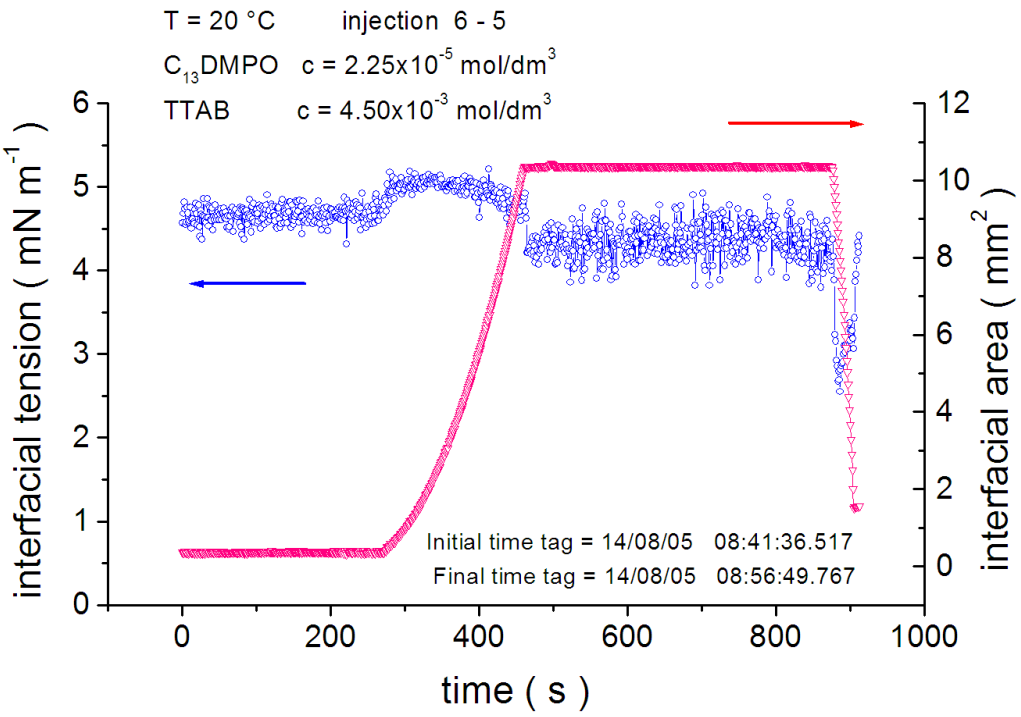


Fig. S2b.- Interfacial tension and interfacial area vs. time for injection 6-5 at T = 20 ℃ for a ramp experiment, including pre-ramp and post-ramp values (with filtered reference pressure and adjusted calibration parameters). The time interval of the ramp is t = 200 s , the selected range for the fit is t = [10 – 180 s ]. The time-origin in the plot has been set arbitrarily at the initial time tag of the experiment.

A satisfactory agreement was observed between the offset value, obtained at the greatest concentration with the corresponding offset at the smallest available surfactant concentration, indicating a calibration stability during the entire microgravity experiments, from July 02 to August 08, 2014. Fig. S3b illustrates an example of a growing drop experiment at temperature T = 20 ℃, for a sample at the smallest available surfactant concentration, i.e., injection 1-1. For this small concentration, a satisfactory comparison of the offset value is observed by taking just the upper extent of the ramp interval, while the interfacial tension matches the interfacial area expansion, as seen in Fig. S4b.

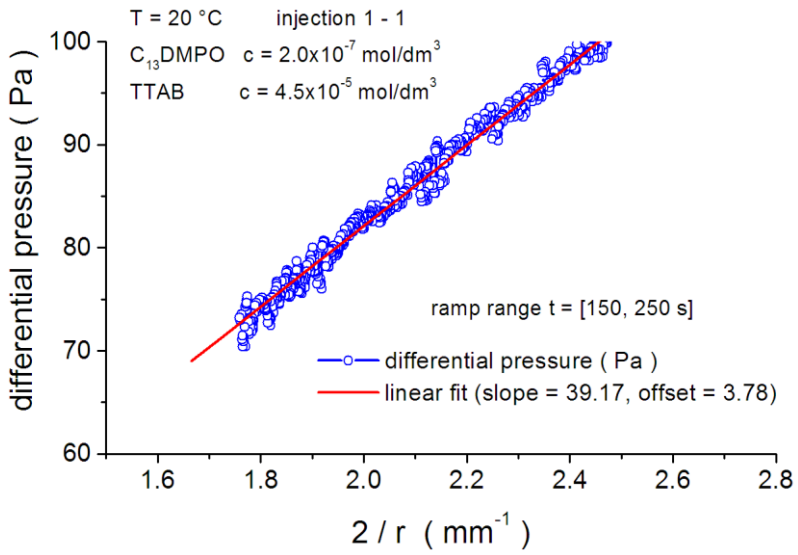


Fig. S3b.- Fitting of differential pressure vs. inverse radius data for injection 1-1 at T = 20 ℃ for a growing drop experiment, where just the upper range of the ramp is selected (results with filtered reference pressure and adjusted calibration parameters).

In addition to the growing drop experiments, Fig. S4b also shows a subsequent step experiment, generating an almost fresh interfacial area. Actually, as seen in the right side of Fig. 4b, in concomitance with the step change of interfacial area, the interfacial tension raises to the value pertinent to pure water/pure n-hexane, around $\gamma$ = 51.1 mN m-1 [ [1b] ], indicating a reliable in-flight calibration.

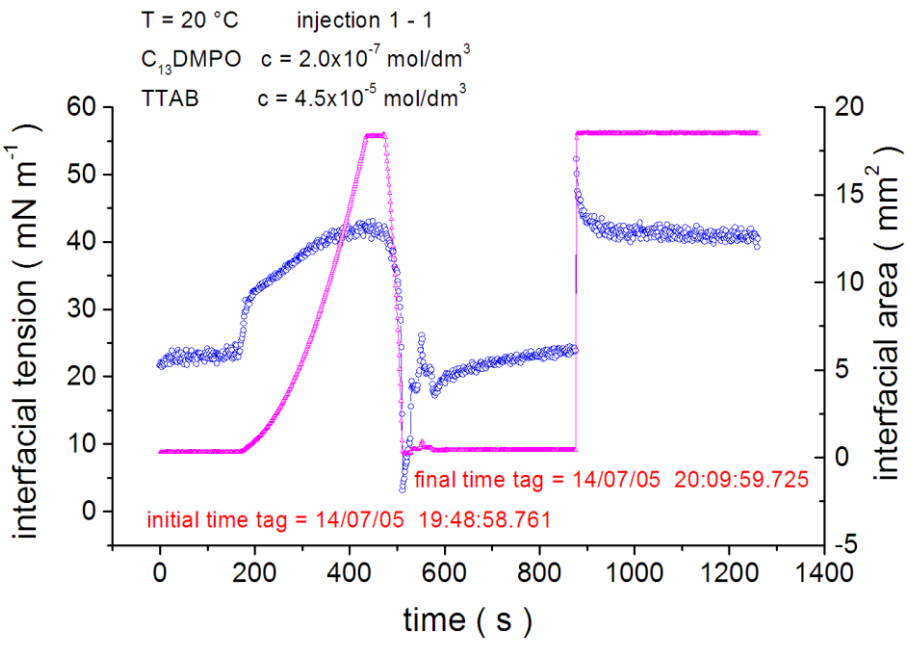


Fig. S4b.- Interfacial tension and interfacial area vs. time for a ramp experiment and for a subsequent step experiment (results with filtered reference pressure and adjusted calibration parameters), for a sample at injection 1-1 and at T = 20 ℃. The time interval of the ramp is t = 250 s , the selected range for the fit is t = [150 – 250 s ].

Reference

[ 1b ] N. Mucic, N.M. Kovalchuk, V. Pradines, A. Javadi, E.V. Aksenenko, J. Krägel, R. Miller, *Dynamic properties of CnTAB adsorption layers at the water/oil interface*, Colloids Surf., A: Physicochem. Eng. Aspects 441 (2014) 825– 830); DOI /10.1016/j.colsurfa.2012.08.071 .

Appendix C

*Data conversion from arbitrary digital units to units of the international system*

Successively to the qualifying items of i) arrangement of data packets in the form of 8-frequency experiment sequences (par. 2.3.), ii) synchronization (paragraph 2.4.), iii) optical calibration check (par. 2.4.1.), iv) pressure calibration adjustment (par. 2.4.2), the telemetered-data files were converted from arbitrary digital-units (DU-units) into units of the international system (SI-units) by the fixed specific calibration factors.

In the course of this conversion, each 1-second packet is split in twenty fractions of second (i.e., $t_n = 0.05 \times n$, n = 0, 1,….19, s) and hence each radius value, r , in each packet was multiplied by half the concomitant differential-pressure value, $\Delta p$ (determining twenty values of the interfacial tension according to the Gauss-Laplace equation). Within the same second, the corresponding interfacial area values, A, were determined via the drop radius values, r, and drop height values, h, according to the proper expression for a spherical cap-shaped drop, i.e, $A = 2\pi r h$.

The effective conversion procedure, applied to all experiment sequences (pertaining to all samples in Tab. 1) resulted in a reliable set of SI-unit values for the interfacial properties (as a function of time, frequency, temperature and concentration) for the studied mixed surfactant systems.

*Frequency domain analysis: measurement value of interfacial dilational viscoelastic modulus*

In the low-frequency range the used algorithm involved the expansion into Fourier series of the oscillation cycles of interfacial tension and area (at 5%, 10% and 20% amplitudes) and subsequent determination of the modulus, i.e. the real part and imaginary part of the interfacial viscoelasticity, according to its definition in the frequency domain [1c]. The properties of the fundamental harmonic are retained for determining the viscoelasticity, while the higher harmonics of the Fourier series expansion (if any) are considered just for the determination of the total harmonic distortion (THD) parameter.

In the high-frequency range the determination of the interfacial viscoelasticity required a specific algorithm, as already described for a similar microgravity experiment [2c].

*Definition of interfacial dilational viscoelastic modulus*

The interfacial dilational viscoelastic modulus is a physical quantity defined in the frequency domain by a complex expression [3c]

$$\varepsilon^*(i\omega) = \varepsilon_r(\omega) + i\,\varepsilon_i(\omega) = \frac{\Delta\gamma \times \exp\left[-i\left(\omega t + \phi\right)\right]}{\Delta A \times \exp\left(-i\omega t\right) / A_0}, \qquad (1c)$$

where ω represents the angular frequency, $\Delta\gamma \times \exp[-i(\omega t + \phi)]$ is the interface response to the imposed area perturbation $\Delta A \times \exp(-i\omega t)/A_0$, $\Delta\gamma$ and $\Delta A$ are the oscillation amplitudes of the interfacial tension and the interfacial area, respectively, $\phi$ the phase shift between perturbation and response, $A_0$ is the mean interfacial area of the sinusoidal cycle, $\varepsilon_r$ and $\varepsilon_i$ are the real and imaginary parts, respectively, of the complex viscoelasticity $\varepsilon^*(i\omega)$.

The definition of $\varepsilon^*(i\omega)$ in Eq.(1c) is extended by the existence of a Fourier transform relationship between the three physical quantities involved in interfacial extension/contraction processes, that is, fractional-area change (time domain), interfacial tension change (time domain) and interfacial dilational modulus (frequency domain) [4c] :

$$\varepsilon^*(i\omega) = \varepsilon_r(\omega) + i\,\varepsilon_i(\omega) = \frac{F\{\Delta\gamma(t)\}}{F\{\Delta A(t)/A_0\}} \qquad (2c)$$

where F is the Fourier transform operator.

The definition of $\varepsilon^*(i\omega)$ , according to Eqs. (1c, 2c), does not require any assumption about the microscopic structure of the studied interface or about the molecular mechanisms occurring in the interfacial layer or in its immediate proximity. The only implicit assumption in Eqs. (1c, 2c) is that the interface behaves as a time-invariant linear system, i.e., that the interface is in adsorption equilibrium condition and it is subjected to small amplitude perturbations.

It is worth noting that the physical quantity $\varepsilon^*(i\omega)$ is a constitutive property of the interfacial systems, taking a definite value at each particular frequency. Actually, $\varepsilon^*(i\omega)$ can be conceived as the transfer function of the interfacial system, connecting the interfacial $\Delta\gamma$ responses to interfacial area perturbations of any functional form in the frequency-domain or in the time-domain. In other words, the definition of $\varepsilon^*(i\omega)$ can be expressed in terms of the $\Delta\gamma$ response to the unit-step function u(t).

Specifically the Fourier transform in the numerator of the ratio in Eq. (2c) reads in explicit integral form:

$$F\{\Delta\gamma(t)\} = \int_0^\infty \Delta\gamma(t) \times e^{-i\omega t}\, dt \qquad (3c)$$

and the analytical expression of the unit-step function, u(t), in the denominator reads:

$$F\{u(t)\} = \pi\delta(\omega) + \frac{1}{i\,\omega} \qquad (4c)$$

where $\delta(\omega)$ is the Dirac delta function.

Hence, combining Eq. (3c) and Eq. (4c) into Eq. (2c) and applying the Euler identity, the values of the real and the imaginary part of $\varepsilon^*(i\omega)$ can be interpreted as the integration values of the $\Delta\gamma(t)$ relaxation function excited by a unit step change of fractional area:

$$\varepsilon^*(i\omega) = i\omega \times F\{\Delta\gamma(t)\} = -\omega\int_0^\infty \Delta\gamma_n(t)\sin(\omega t)dt + i\omega\int_0^\infty \Delta\gamma_n(t)\cos(\omega t)dt \qquad (5c)$$

where the relaxation function is normalized as $\Delta\gamma_n(t) = \Delta\gamma(t)/(\Delta A/A_0)$ [4c].

Moreover, a static elasticity constant value, $E_0$, must be added to Eq. (5c) when the interfacial layer contains a component which is insoluble in both adjoining phases at the interface [5c].

The expression of Eq. (5c), as for the case of Eq. (2c), is valid whatever is the mechanism at the molecular level which generates the observable interfacial viscoelasticity phenomenology.

The definition of ε*(iω) in Eqs. (1c, 2c, 5c) still holds in nonideal initial adsorption equilibrium provided that the $\Delta\gamma_n(t)$ relaxation function vanishes at zero value in a time interval at least one order of magnitude shorter than the time-interval of the nonequilibrium condition evolution, at the start of the interfacial layer excitation.

In fast dynamic nonlinear condition, the interface anyway shows a viscoelastic behavior, but a modulus cannot be correctly defined, being the viscoelastic property instead conveniently described by Lissajous curves [6c].

*Case of diffusion-controlled adsorption*

When the normalized relaxation function $\Delta\gamma_n(t)$ has the particular form of the Sutherland equation [7c]

$$\Delta\gamma_n(t) \;=\; \varepsilon_0 \;\exp(2\omega_0 t)\, erfc(2\omega_0 t)^{1/2} \tag{6c}$$

then the integral expression in Eq. (5c) constitutes a transformed representation of the Lucassen model for the diffusion controlled adsorption mechanism:

$$\varepsilon_r = \frac{\varepsilon_0\,[1+\,(\omega_0/\omega)^{0.5}\,]}{1+2\,(\omega_0/\omega)^{0.5}+2\,\omega_0/\omega} \tag{7c}$$

$$\varepsilon_i = \frac{\varepsilon_0\,[\,(\omega_0/\omega)^{0.5}\,]}{1+2\,(\omega_0/\omega)^{0.5}+2\,\omega_0/\omega} \tag{8c}$$

Actually the Sutherland equation, Eq. (6c), is essentially the step response decay function that can be derived from the Fourier-transform expression in Eq. (2c), by insertion of ε*(iω) in the form of the Lucassen model for the diffusional exchange at the interfacial layer, i.e., Eqs. (7c, 8c) [8c].

*Case of Maxwell-model relaxation function*

The generalized Maxwell model is usefully applied to calculate the relaxation time spectra for multicomponent interfacial layers as well as for commercial mixtures of surfactants [9c]. A single element of the Maxwell model is constituted by an elastic spring and a viscous dash-pot in series, with parameters k and η, respectively. Then the expression for the complex viscoelastic modulus is obtained by inserting in Eq. (5c) the Maxwell-model relaxation function of the interfacial tension, excited by a unit step change of fractional area:

$$\varepsilon^*(i\omega) \;=\; -\omega\int_0^\infty \Delta\gamma_n(0)\, e^{-kt/\eta}\sin(\omega t)dt + i\omega\int_0^\infty \Delta\gamma_n(0)\, e^{-kt/\eta}\cos(\omega t)dt \tag{9c}$$

Upon integration of Eq. (9c), the real part of the complex modulus reads

$$\varepsilon_r = \frac{\Delta\gamma_n(0)\times\omega^2}{(\kappa/\eta)^2+\omega^2} \tag{10c}$$

and the imaginary part reads

$$\varepsilon_i = \frac{\Delta\gamma_n(0)\times\omega\times(\kappa/\eta)}{(\kappa/\eta)^2+\omega^2} \tag{11c}$$

References

[1c] G. Loglio, P. Pandolfini, L. Liggieri, A.V. Makievski, F. Ravera, Determination of interfacial properties by the pendant drop tensiometry: optimization of experimental and calculation procedures, in Bubble and Drop Interfaces, “Progress in Colloid and Interface Science” Series, L. Liggieri and R. Miller (Eds.), Volume 2, Chapter 2, pp. 7-38, Brill, Leiden, the Netherlands, 2011.

[2c] P. Pandolfini, G. Loglio, F. Ravera, L. Liggieri, V.I. Kovalchuk, A. Javadi, M. Karbaschi, J. Kr ägel, R. Miller, B.A. Noskov, A.G. Bykov, Dynamic properties of Span-80 adsorbed layers at paraffin-oil/water interface: Capillary pressure experiments under low gravity conditions, Colloids Surf. A: Physicochem. Eng. Aspects, 532 (2017) 228-243.

[3c] J. Lucassen, M. van den Tempel, Dynamic measurements of dilational properties of a liquid interface, Chem. Eng. Sci., 27 (1972) 1283-1291.

[4c] G. Loglio, U. Tesei, R. Cini, Spectral Data of Surface Viscoelastic Modulus Acquired via Digital Fourier Transformation, J. Colloid Interface Sci. 71 (1979) 316-320.

[5c] B.A. Noskov, G. Loglio, Dynamic surface elasticity of surfactant solutions, Colloids Surf. A: Physicochem. Eng. Aspects, 143 (1998) 167–183 .

[6c] A.G. Bykov, L. Liggieri, B.A. Noskov, P. Pandolfini, F. Ravera, G. Loglio, Surface dilational rheological properties in the nonlinear domain, Adv. Colloid Interface Sci., 222 (2015) 110-118 .

[7c] K.L. Sutherland, The kinetics of adsorption at liquid surfaces, Austr. J. Sci. Res. , A5 (1952) 683- 696.

[8c] G. Loglio, E. Rillaerts, P. Joos, Fourier transform surface viscoelastic modulus of dilute aqueous solutions of surfactants. Improved computational methods, Colloid Polym. Sci,, 259 (1981) 1221-1227.

[9c] S. D. Rosales-Anzola, M. Garc á-Sucre, G. Urbina-Villalba, E. Lopez, Surface dilational viscoelasticity of surfactants, in "Topics in the Colloidal Aggregation and Interfacial Phenomena", (M. Garcia-Sucre, A. Loszan, A. J. Castellanos-Suarez, J. Toro-Mendoza, Eds.), Chapter 7, ISBN: 978-81-308-0491-0, 2012, Research Signpost, Kerala, India.

Appendix D

*The surface dilational viscoelasticity of an oil-water interface with two surfactants soluble in both oil and water*

If there are two surfactants that are distributed between two immiscible liquids (e.g. oil and water), separated by a flat interface, then the variation of their concentrations under dynamic conditions is described by the set of Fick's equations

$$\frac{\partial c_j^{\alpha}}{\partial t} = D_j^{\alpha} \frac{\partial^2 c_j^{\alpha}}{\partial x^2}, \qquad x > 0 \qquad (j = 1, 2) \tag{1d}$$

$$\frac{\partial c_j^{\beta}}{\partial t} = D_j^{\beta} \frac{\partial^2 c_j^{\beta}}{\partial x^2}, \qquad x < 0 \qquad (j = 1, 2) \tag{2d}$$

where $c_j^{\alpha,\beta}$ and $D_j^{\alpha,\beta}$ are the concentration and diffusion coefficient of the jth surfactant in the phases $\alpha$ and $\beta$, respectively, t is the time, and x is the coordinate normal to the interface, located at $x = 0$ . We will consider a local equilibrium state at the interface when the concentrations in the two phases close to the interface (subsurface concentrations) $c_{Sj}^{\alpha} = c_j^{\alpha}\big|_{x=+0}$ and $c_{Sj}^{\beta} = c_j^{\beta}\big|_{x=-0}$ are related via the equilibrium distribution coefficient

$$K_j = \frac{c_{Sj}^{\beta}}{c_{Sj}^{\alpha}}, \qquad x = 0 \qquad (j = 1, 2) \tag{3d}$$

This equation is the first boundary condition for the set of equations Eqs. (1d) and (2d). The second boundary condition reflects the surfactants' balance at the interface, accounting for the diffusional exchange between the interface and the two adjacent liquid phases

$$\frac{1}{A}\frac{d(\Gamma_j A)}{dt} = \frac{d\Gamma_j}{dt} + \frac{\Gamma_j}{A}\frac{dA}{dt} = D_j^{\alpha}\frac{\partial c_j^{\alpha}}{\partial x}\bigg|_{x=+0} - D_j^{\beta}\frac{\partial c_j^{\beta}}{\partial x}\bigg|_{x=-0}, \qquad x = 0 \qquad (j = 1, 2) \tag{4d}$$

where $\Gamma_j$ are the surfactants adsorptions at the interface, A is the area of the interface. Two additional boundary conditions are:

$$c_j^{\alpha} \to c_{0j}^{\alpha}, \qquad x \to +\infty \qquad \text{and} \qquad c_j^{\beta} \to c_{0j}^{\beta}, \qquad x \to -\infty \qquad (j = 1, 2) \tag{5d}$$

where $c_{0j}^{\alpha}$ and $c_{0j}^{\beta}$ are the equilibrium concentrations. For established harmonic oscillations of the interface, periodicity of concentration variations can serve as initial conditions:

$$c_j^{\alpha,\beta}(t) = c_j^{\alpha,\beta}\left(t + \frac{2\pi}{\omega}\right) \qquad (t = 0) \qquad (j = 1, 2) \tag{6d}$$

where $\omega$ is the radial frequency of the oscillations. The general solutions of Eqs. (1d) and (2d) satisfying the boundary conditions Eq. (5d) and the initial conditions Eq. (6d) have the form

$$c_j^{\alpha} = c_{0j}^{\alpha} + E_j^{\alpha}\, exp\left(-(1+i)\sqrt{\frac{\omega}{2D_j^{\alpha}}}x\right)e^{i\omega t} \tag{7d}$$

$$c_j^\beta = c_j^\beta + E_j^\beta \, exp\left( (1+i)\sqrt{\frac{\omega}{2D_j^\beta}}x \right) e^{i\omega t} \tag{8d}$$

where $E_j^\alpha$ and $E_j^\beta$ are the unknown integration constants. With these solutions, from the boundary condition Eq. (3d) one obtains

$$c_{0j}^\beta + E_j^\beta e^{i\omega t} = K_j c_{0j}^\alpha + K_j E_j^\alpha e^{i\omega t} \tag{9d}$$

With account for the equilibrium conditions $c_{0j}^\beta = K_j c_{0j}^\alpha$ this leads to

$$E_j^\beta = K_j E_j^\alpha \tag{10d}$$

This allows to exclude two unknown integration constants. To determine the remaining two integration constant one has to use the boundary conditions Eq. (4d). For small-amplitude harmonic oscillations of the interface the surface area variation can be expressed as

$$A = A_0 + \Delta A_0 e^{i\omega t} \tag{11d}$$

where $A_0$ is the equilibrium surface area and $\Delta A_0$ is the amplitude of the surface area variation. Then the boundary conditions Eq. (4) yield

$$\frac{d\Gamma_j}{\partial t} + \frac{\Gamma_{0j}}{A_0}\frac{dA}{dt} = D_j^\alpha \frac{\partial c_j^\alpha}{\partial x}\bigg|_{x=+0} - D_j^\beta \frac{\partial c_j^\beta}{\partial x}\bigg|_{x=-0} \tag{12d}$$

where $\Gamma_{0j}$ are the equilibrium adsorptions. Taking into account that the adsorptions are also harmonic functions of time $\Gamma_j = \Gamma_{0j} + \Delta\Gamma_j e^{i\omega t}$ and using the solutions Eqs. (7d) and (8d) one obtains

$$i\omega\Delta\Gamma_j e^{i\omega t} + i\omega\frac{\Gamma_{0j}}{A_0}\Delta A_0 e^{i\omega t} = -D_j^\alpha E_j^\alpha (1+i)\sqrt{\frac{\omega}{2D_j^\alpha}} e^{i\omega t} - K_j D_j^\beta E_j^\alpha (1+i)\sqrt{\frac{\omega}{2D_j^\beta}} e^{i\omega t} \tag{13d}$$

or

$$\Delta\Gamma_j + (1-i)\sqrt{\frac{D_j^{ef}}{2\omega}} E_j^\alpha = -\frac{\Gamma_{0j}}{A_0}\Delta A_0 \tag{14d}$$

where $D_j^{ef}$ are the effective diffusion coefficients defined as

$$D_j^{ef} = \left( \sqrt{D_j^\alpha} + K_j \sqrt{D_j^\beta} \right)^2 \tag{15d}$$

In mixed adsorption layers comprising two surfactants the adsorptions are functions of the two surfactant concentrations: $\Gamma_j = \Gamma_j\left(c_{S1}^\alpha, c_{S2}^\alpha\right)$, therefore the variations of adsorptions can be written as

$$\Delta\Gamma_j = a_{j1} E_1^\alpha + a_{j2} E_2^\alpha \tag{16d}$$

where $a_{11} = \left(\frac{\partial\Gamma_1}{\partial c_{S1}^\alpha}\right)_{c_{S2}^\alpha}$, $a_{12} = \left(\frac{\partial\Gamma_1}{\partial c_{S2}^\alpha}\right)_{c_{S1}^\alpha}$, $a_{21} = \left(\frac{\partial\Gamma_2}{\partial c_{S1}^\alpha}\right)_{c_{S2}^\alpha}$ and $a_{22} = \left(\frac{\partial\Gamma_2}{\partial c_{S2}^\alpha}\right)_{c_{S1}^\alpha}$. In Eq. (16d) the adsorptions are considered as functions of the surfactant concentrations in the phase $\alpha$, however they can be also considered as functions of the concentrations in the phase $\beta$, i.e. $\Gamma_j = \Gamma_j\left(c_{S1}^\beta, c_{S2}^\beta\right)$, because the concentrations on both sides of the interface are related via the equilibrium distribution coefficients, Eq. (3d).

Eqs. (14d) and (16d) form a set of four linear equations with respect to the four unknown amplitudes: two $E_j^{\alpha}$ and two $\Delta\Gamma_j$. Following standard procedures one obtains

$$E_1^{\alpha} = -\frac{\Gamma_{01}a_{22}\left(1+(1-i)\zeta_2\right)-\Gamma_{02}a_{12}}{a_{11}a_{22}\left(1+(1-i)\zeta_1\right)\left(1+(1-i)\zeta_2\right)-a_{12}a_{21}}\frac{\Delta A_0}{A_0} \tag{17d}$$

$$E_2^{\alpha} = -\frac{\Gamma_{02}a_{11}\left(1+(1-i)\zeta_1\right)-\Gamma_{01}a_{21}}{a_{11}a_{22}\left(1+(1-i)\zeta_1\right)\left(1+(1-i)\zeta_2\right)-a_{12}a_{21}}\frac{\Delta A_0}{A_0} \tag{18d}$$

$$\Delta\Gamma_1 = -\frac{\Gamma_{01}\left(a_{11}a_{22}-a_{12}a_{21}+(1-i)\zeta_2 a_{11}a_{22}\right)+\Gamma_{02}(1-i)\zeta_1 a_{11}a_{12}}{a_{11}a_{22}\left(1+(1-i)\zeta_1\right)\left(1+(1-i)\zeta_2\right)-a_{12}a_{21}}\frac{\Delta A_0}{A_0} \tag{19d}$$

$$\Delta\Gamma_2 = -\frac{\Gamma_{02}\left(a_{11}a_{22}-a_{12}a_{21}+(1-i)\zeta_1 a_{11}a_{22}\right)+\Gamma_{01}(1-i)\zeta_2 a_{21}a_{22}}{a_{11}a_{22}\left(1+(1-i)\zeta_1\right)\left(1+(1-i)\zeta_2\right)-a_{12}a_{21}}\frac{\Delta A_0}{A_0} \tag{20d}$$

where $\zeta_1 = \sqrt{\frac{D_1^{ef}}{2(a_{11})^2\omega}} = \sqrt{\frac{\omega_{D1}}{2\omega}}$ and $\zeta_2 = \sqrt{\frac{D_2^{ef}}{2(a_{22})^2\omega}} = \sqrt{\frac{\omega_{D2}}{2\omega}}$ are the dimensionless variables and $\omega_{D1} = \frac{D_1^{ef}}{(a_{11})^2}$ and $\omega_{D2} = \frac{D_2^{ef}}{(a_{22})^2}$ are the characteristic relaxation frequencies. The surface dilational viscoelastic modulus can be written as

$$\varepsilon = -\varepsilon_{01}\frac{d\,ln\,\Gamma_1}{d\,ln\,A} - \varepsilon_{02}\frac{d\,ln\,\Gamma_2}{d\,ln\,A} \approx -\varepsilon_{01}\frac{A_0\Delta\Gamma_1}{\Gamma_{01}\Delta A} - \varepsilon_{02}\frac{A_0\Delta\Gamma_2}{\Gamma_{02}\Delta A} \tag{21d}$$

where $\varepsilon_{01} = -\left(\frac{\partial\gamma}{\partial\, ln\,\Gamma_1}\right)_{\Gamma_2,T}$ and $\varepsilon_{02} = -\left(\frac{\partial\gamma}{\partial\, ln\,\Gamma_2}\right)_{\Gamma_1,T}$ are the partial elasticities, as defined by Joos [1d]. Then, using Eqs. (19d), (20d) and (21d) one obtains

$$\varepsilon = \frac{\varepsilon_{01}}{Z}\left[1-\frac{a_{12}a_{21}}{a_{11}a_{22}}+(1-i)\zeta_2+\frac{\Gamma_{02}}{\Gamma_{01}}(1-i)\zeta_1\frac{a_{12}}{a_{22}}\right]+\frac{\varepsilon_{02}}{Z}\left[1-\frac{a_{12}a_{21}}{a_{11}a_{22}}+(1-i)\zeta_1+\frac{\Gamma_{01}}{\Gamma_{02}}(1-i)\zeta_2\frac{a_{21}}{a_{11}}\right] \tag{22d}$$

where $Z = \left(1+(1-i)\zeta_1\right)\left(1+(1-i)\zeta_2\right)-\frac{a_{12}a_{21}}{a_{11}a_{22}}$.

Thus, the surface dilational viscoelastic modulus of a surfactant mixture depends on two characteristic frequencies, $\omega_{D1}$ and $\omega_{D2}$, which characterize the rates of diffusional relaxation of the two surfactants in the mixture. These characteristic frequencies are determined by the effective diffusion coefficients $D_1^{ef}$ and $D_2^{ef}$, which depend on the diffusion rate in both liquid phases. The effective diffusion coefficients depend also on the surfactants' distribution coefficients $K_j$. The diffusion in a phase, where the surfactant is more soluble, is more important for the surface dilational viscoelastic modulus. The surface dilational viscoelastic modulus of a mixture depends also on some equilibrium parameters: $\varepsilon_{0j}$, $\Gamma_{0j}$ and the ratios $a_{12}/a_{22}$ and $a_{21}/a_{11}$. If the second surfactant is absent, $c_{02}^{\alpha} = c_{02}^{\beta} = 0$, then $\varepsilon_{02} = 0$, $\Gamma_{02} = 0$ and $a_{21} = 0$, and we obtain from Eq. (22d) the classical Lucassen/van den Tempel equation:

$$\varepsilon = \frac{\varepsilon_{01}}{1+(1-i)\zeta_1} = \varepsilon_{01}\frac{1+\zeta_1+i\zeta_1}{1+2\zeta_1+2\zeta_1^2} \tag{23d}$$

Eq. (22d) can be transformed to a form similar to that derived previously by Jiang et al. [2d]. However, these authors considered a system of two surfactants dissolved only in one liquid. In our case we have two surfactants dissolved in two liquids. This leads to the appearance of the effective diffusion coefficients $D_1^{ef}$ and $D_2^{ef}$ instead of the usual diffusion coefficients $D_1$ and $D_2$.

[1d] P. Joos, Dynamic Surface Phenomena, VSP, Dordrecht, The Netherlands, 1999.

[2d] Q. Jiang, J.E. Valentini, Y.C. Chiew, Theoretical models for dynamic dilational surface properties of binary surfactant mixtures. J. Colloid Interface Sci. 174 (1995) 268-271.